SLAC/AP--16

DE84 012498

SLAC/AP-16

February 1984

HIGH-GRADIENT, PULSED OPERATION OF SUPERCONDUCTING NIOBIUM CAVITIES*

ISIDORO E. CAMPISI AND Z. DAVID FARKAS

Stanford Linear Accelerator Center

Stanford University, Stanford, California 94305

ABSTRACT

Tests performed on several Niobium TM_{010} cavities at frequencies of about 56 MHz using a high-power, pulsed method indicate that, at the end of the arging pulse, peak surface magnetic fields of up to ~ 1300 Oe, corresponding a peak surface electric field of ~ 68 MV/m, can be reached at 4.2°K without preciable average losses. Further studies of the properties of superconductors der pulsed operation might shed light on fundamental properties of RF superductivity, as well as lead to the possibility of applying the pulse method to e operation of high-gradient linear colliders.

Work supported by the Department of Energy, contract DE-AC03-76SF00515

1. Introduction

The operation of superconducting cavities with short pulses is not a totally new technique. Other experimenters have used it occasionally, but more as an incidental observation tool, than a systematic way of testing properties of superconductors or for possible practical applications.[1,2]

At SLAC tests of superconducting cavities using high-power, short-pulse klystrons as power sources were started in the Spring of 1982 as a by-product of pulsed RF processing to possibly increase the breakdown fields in cw-operated cavities.

At that time one of us (ZDF) derived in detail how the cavity should be coupled to the transmission line in order to achieve the maximum possible energy transfer efficiency of the RF pulse. Those derivations are contained in a separate report.[3]

The pulsed RF processing did indeed improve the cw field at which the Q_0 degradation starts, up to $\sim$ 20 MV/m from $\sim$ 16 MV/m prior to processing, at a temperature of $\sim$ 1.4°K. These tests were performed on only one Nb cavity.

One high-power, pulsed test was performed at that time at 4.2°K and a quick analysis of the few data taken indicated then that a peak surface electric field of $E_p \sim 50$ MV/m ($H_p \sim 950$ Oe) could be reached without appreciable Q_0 degradation.

Since then a more thorough series of tests was performed in January 1983 on the same cavity with the variable coupling system originally designed for the low-power, cw operation. The analysis of the data then performed confirmed the result of $\sim$ 50 MV/m [4] and reinforced the opinion that the original cause of Q

degradation lied in the coupling system and not in the cavity proper.[5]

It was then decided that the construction of a new fixed-coupling system designed for high-power operation was necessary, but at the same time it was clear that even larger field gradients could possibly be achieved with Nb_3Sn,[6] which could lead to practical applications in high-energy electron linear colliders.

In view of this possibility, a collaboration with the University of Wuppertal (Professor H. Piel, Dr. G. Arnolds-Mayer) was started: their production of Nb_3Sn cavities, obtained by Sn vapor deposition techniques,[7] has proved to be consistently good [Q_0 (4.2°K)$\gtrsim 5 \times 10^9$, E_a(cw) $\simeq$ 8 MV/m].

A number of Nb cavities with fixed coupling was then manufactured for the purpose of coating them with Nb_3Sn. The cavities were originally manufactured through a coining process at SLAC about ten years ago as cavity halves for the LEAPFROG project; five of them were assembled and tested both with the low-power, cw method and with the high-power pulsed method. The rest of this note describes in detail the experiment and the results of those measurements.

2. Optimum Energy Transfer of an RF Pulse to a Resonator

The energy transfer efficiency η of an RF pulse into a cavity is given by[4]

$$\eta = \frac{\alpha[(1-e^{-\tau_p})]^2}{\tau_p} \tag{1}$$

where $\alpha = 2/(1+Q_e/Q_0)$, $\tau_p = T_p/T_c$, T_p is the RF pulse length, $T_c = \alpha Q_e/\omega$.

For a cavity with negligible losses ($Q_0 \gg Q_e, Q_e \simeq Q_L$), η is a maximum for

$$Q_e = 2.5/\ T_p \tag{2}$$

where f is the frequency of the RF.

Figure 1 illustrates the behavior of the reverse power for a pulse length of 2.5 μs and for the optimum Q_e and for Q_e half and twice that value.

Figure 2 gives the energy transfer efficiency for the pulse lengths of 1 and 2.5 μs as a function of external Q. For optimum coupling this efficiency is close to 80% and does not vary appreciably for less-than-optimum coupling over a fairly large range of coupling.

3. Determination of Peak Fields in the Cavity Through Average Power Measurements

In general, the peak surface electric field in a resonator can be determined from the knowledge of the energy stored in it as

$$E_s = k\sqrt{U_s} \tag{3}$$

where k is a numerical coefficient determined by the cavity geometry and which can be obtained by standard LALA or SUPERFISH computer programs.

The coefficients for the two types of cavities that we have tested are: $k = 76$ MV/(m$\sqrt{J}$) and for the SLAC cavity (Fig. 10) and $k = 78.6$ MV/(m$\sqrt{J}$) for the LEAPFROG cavities (Fig. 11). In the steady-state condition the energy stored is determined as a function of incident power P_i, unloaded quality factor Q_0, radian frequency ω and coupling β, as

$$U_{cw} = \frac{P_i Q_0}{\omega} \frac{4\beta}{(1+\beta)^2} \tag{4}$$

In the pulsed operation the stored energy reaches a maximum at the end of the pulse. Then it decays with a time constant $2Q_L/\omega$. In the low-loss condition the power instantaneously emitted during the decay can be integrated, and the value of the integral gives the energy stored in the cavity at the inception of the decay:

$$U_s = \int_{T_p}^{\infty} P_e(t)\,dt \qquad (5)$$

In the general case the stored energy is the sum of the energy emitted and the energy dissipated during discharge: this second term is Q_e/Q_0 times smaller than the first and can be neglected in our case.

An average power meter automatically performs the integration not only over the decay time, but also over the number of pulses delivered per unit time (PRF), as long as only the portion of the reflected power emitted after the end of the RF pulse is allowed to reach the meter itself (Fig. 3). Therefore:

$$U_s = \frac{P_e}{\mathrm{PRF}} \simeq U_s \qquad (6)$$

By taking into account the attenuation factors between the cavity and the power meter sensor, we can determine the peak surface electric field reached in the cavity from measurable quantities as

$$E_s = k\sqrt{\frac{P_e}{\mathrm{PRF}}} \qquad (7)$$

It should be noted that when the approximation $Q_0 \gg Q_e$ breaks down as the losses increase, the average power method gives a lower limit to the estimate of the fields in the cavity at the beginning of the decay. Since this method

integrates the power under the decay curve, for a faster decay than in the ideal case ($Q_L < Q_e$) the initial power emitted must be higher to give the same integral.

4. Experimental Apparatus

The measuring system for the pulsed tests is shown in Fig. 4. In this scheme we also show the timing systems to the various components of the RF amplifiers, because through them we are able to vary the repetition rate and the length of the RF pulse.

The cavity is decoupled from the klystron via an evacuated waveguide 7 dB coupler, in order to avoid damage to the klystron due to power reflection. The incident and reflected powers are sampled using a 56.3 dB cross-guide coupler; isolators and band pass filters are also employed before the power is detected by the power meters' thermocouple sensors. The sensors' power calibration is rated close to 1% error.

The reflected signal goes through a PIN diode modulator gated by a pulse generator, part of the signal is then detected by a crystal rectifier and observed on a scope, in order to set the gate at the appropriate time at the end of the pulse. The fraction of the power past the end of the RF pulse is then measured by the average power meter.

4.1 Power Calibration Procedure

The major source of error in the absolute power measurements must be ascribed to the calibration of the losses in the part of the microwave circuit from the reflected power arm of the cross guide coupler to the power meter. The calibration is done in two steps: first the attenuation of the filters and isolator assembly

is measured at the output of a low-power, voltage-controlled oscillator at the cavity operating frequency, then the assembly is connected to the waveguide-to-N type adaptor, and the power measured again past the filters and isolators. Finally the PIN diode modulator is connected with the gate fully open and the attenuation through modulator and coupler measured. The largest uncertainly in the measurements (usually of up to ±2% in power) is related to making and breaking cable connections in the process of performing the attenuation measurements. This process has been repeated several times: in most instances the differences in attenuation were limited to about 1%, but in a couple of occasions these differences amounted to up to 8%. It should be pointed out, though, that when the attenuation was consistently stable it was also in agreement with the input power attenuation, while in those few occasions when it departed from the normal value it was always larger than usual, and gave lower power reading than normal. Since the measurements always used the emitted power for the absolute determination of the fields, it turns out that our figures are, in the worst case, a lower limit to the actual likely values, with a maximum 5% error in power.

4.2 Other Instruments and Apparatus

A transmission probe is also available, which allows us to monitor the fields in the cavity using a linear IF amplifier and a logarithmic amplifier as well: the logarithmic amplifier ensured us that during the decay the fields were decreasing exponentially, both below and above the threshold for increased losses in the cavity (Fig 6). The linear amplifier, on the other hand, gave us a good indication of the peak field behavior of the cavity (Fig. 7). Although the signal through the amplifier has not yet been calibrated, it is in principle possible to determine the peak fields in the cavity by measuring the peak voltage of the linear amplifier. In

one instance the amplifier was calibrated at field levels well below breakdown and it was possible to establish that up to breakdown the integrated energy method and the peak field method were in excellent agreement, while after breakdown the peak field data were giving higher readings, as they should, since the integral method approach gives lower estimates of the peak fields as the approximation $Q_0 \gg Q_e$ breaks down. A first order approximation correction to the integral method, to be discussed below, gives better agreement between the two results.

Scintillator-phototube assemblies were positioned one on the top of the dewar along the cavity axis and the other outside the dewar at the cavity's equatorial plane. The two tubes had been set for equal signal amplitude and their output was monitored in synchronism with the RF pulse (Fig. 8). The tubes have not yet been calibrated in energy because the signal from the cavity is typically concentrated in a .5 μs time: the possibility exists that, due to their large number, the photon pulses could ride on top of each other, thus giving spurious energy readings. Steps are under way to reduce the photon flux to the photomultiplier assembly in order to calibrate and correlate the maximum photon energy to the field amplitude in the cavity.

Observation of the signal from the photomultipliers has in any case determined that the photons are predominantly emitted along the equatorial plane, consistent with a nonrelativistic bremsstrahlung emission from electrons accelerated along the cavity axis.

An x-ray survey meter was also available just outside the dewar to monitor the integrated x-ray emission rate from the cavity. Signals as high as several hundreds mR/hr were detected at the inception of breakdown of some cavities, while beyond breakdown several R/hr were observed. It should be pointed out

that the RF duty cycle was typically less than 10^{-4}, so that, while emitting x-rays, the cavity was producing an equivalent continuous intensity of several thousands R/hr.

A Helium boiloff gauge was also available to monitor the breakdown at 4.2°K. The laminary-flow element manometer has a resolution of about .02 ℓ/hr of Helium boiloff. Since a thermal load of 1 W gives an increase in boiloff rate of about 1.2 ℓ/hr, the resolution in power is close to 15 mW.

The exact expression for the energy dissipated in the cavity per pulse, U_d, is given in Ref. 1. For a pulse width approximately equal to or less than the cavity time constant, the energy dissipaterd during charging is $(U_s/3)(\omega/Q_0)$. For $\beta \gg 1$ the energy dissipated during discharge is U_s/β. Therefore the Q_0 averaged over a pulse can be expressed as

$$Q_0 \simeq \eta \left[\frac{\omega T_p}{3} + Q_e\right] \frac{P_i}{P_d} \quad , \tag{8}$$

or

$$Q_0 \simeq \eta \left[\frac{\omega T_p}{3} + \frac{\omega T_p}{2.51}\right] \frac{P_i T_p \mathrm{PRF}}{P_d} \quad , \tag{9}$$

where η is the pulse energy transfer efficiency (typically .7-.8), P_i is the average incident power, P_i is the peak incident power of the RF pulse, PRF is the pulse repetition frequency and P_d is the average power dissipated into the bath. For $P_d = 15$ mW we obtain the minimum Q_0 which can be detected as ($\omega = 2\pi \times 2.85 \times 10^9\ \mathrm{s}^{-1}$, $T_p = 2.5\ \mu\mathrm{s}$)

$$Q_{0\mathrm{thr}} \simeq 4.2 \times P_i \times \mathrm{PRF} \quad , \tag{10}$$

where P_i is measured in watts. At the level where the cavity Q starts to degrade ($E_s \simeq 60$ MV/m) P_i is approximately 2.5×10^6 W. Tests conducted at about

PRF = 50-80 pps give a $\bar{Q}_0$ as high as 8×10^7 at the treshold for degradation, in fair agreement with the CW low power Q_0's measured at 4.2°K of $\sim 10^8$.

It should be pointed out that, although the average $\bar{Q}_0$ determined in this way does not give the losses as a function of peak field during the pulse, nonetheless is of importance for practical applications, since it gives an idea of the refrigerator power necessary to achieve a given peak field in the cavity. Full calculations of the nonlinear losses in the cavity during the pulse will be necessary to correctly evaluate the instantaneous Q_0 as the cavity is charging and discharging.

5. Cavity Description and Results of Measurements

A total of five Nb cavities have been tested so far at high power. A sixth cavity has been tested, together with the others, at low power: its frequency is at the moment too low for a high power test, since it falls outside the bandwidth of the 24 MW klystron amplifier.

The cross section of the SLAC-Type TM_{010} cavity, which was built in 1971, is shown in Fig. 9. The cavity was modified for fixed-coupling operation by removing one of the cutoff tubes and adding a double flange system which allows operation with the variable-coupling probe (Fig. 10). The same cutoff tube was used in testing the other five cavities in the CW mode. These cavities were manufactured approximately ten years ago (LEAPFROG project) and they were modified and assembled with a fixed-coupling iris (Figs. 11 and 12). It should be pointed out that the design of the coupling iris was made by having in mind, as the primary objective, the elimination of the coaxial variable coupling mechanism, unreliable at high-power. It was clear that the adopted design did present problems with the iris cooling, especially at temperatures higher that

the λ point. It was nonetheless felt that the design was adequate for the present tests and only in subsequent applications a more efficient way of cooling would be necessary. The cavities were electron-beam welded, fired at 1950°C for 3 hours in ultra-high vacuum. Some of them were lightly etched after a first test, to remove Nb droplets spattered in the welding process.

5.1 Low-Power, CW Tests

Tests at low power with the long pulse method gave a wide range of results both for maximum Q_0 and maximum peak surface field before breakdown (see Table I). Also the types of breakdown varied from cavity to cavity. The SLAC cavity, LEAPFROG1 (LF1) and LF4 gave repetitive quenches at relatively high fields ($E_p > 20$ MV/m) during operation at 1.4°K, with strong x-ray emission, while the others were thermally loaded by the existence of bad spots and Nb droplets.

The SLAC cavity had a performance similar to that measured during the previous tests, indicating that the surgery performed on it, as well as the existence of an additional joint at the cutoff tube flange, did not appreciably affect the performance.

Also, the SLAC cavity was tested twice: as it came out of the firing process and after it had gone through the chemical Indium removal procedure. This second set of tests indicated that the Indium stripping greatly affected the cavity performance at CW, as the Q_0 dropped significantly after the chemical treatment. More significantly, the peak surface field dropped by a factor of two, and the breakdown mechanism shifted from quenching to slow thermal Q_0 degradation during the long pulse. This test confirmed the fact that, for the CW cavity performance, great care is necessary in the treatment of the surfaces. None of

the other cavities were treated for Indium removal, but some of them were etched after a first test, because of the spattered Nb droplets.

5.2 High-Power Test Results

Five of the six cavities have been tested with the short-pulse, high-power method for a variety of temperatures, pulse lengths and repetition rates.

A number of curves showing the average gated emitted power as a function of the average incident power have been produced. These curves proved to be extremely useful in characterizing the cavity behavior, especially in identifying the field level at which the losses start to increase, indicating that the superconductor's surface losses are beginning to increase.

The curve P_e vs P_i is a straight line up to the point where losses start to become significant: at this point the curve bends and, depending on repetition rate, pulse length and temperature, it can assume a variety of behaviors which are related to the fundamental physical processes in the superconductor, but convolved with more mundane properties of the cavity, such as the field-emitted electrons heating the surface, the heat transfer properties to the bath, the existence of bad spots and so on. Figures 13-17, give an idea of some of the shapes of these curves, with various parameters and various cavities. The P_e vs P_i curves are obtained by slowly varying the incident peak power, both upward and downward. The curves can be reproduced very closely if the process is repeated several times.

Hysteretic thermal degradations of Q_0, associated with the thermal properties of the cavity and the Nb-He interface, have been observed with a variety of substructures which might shed light on the loss mechanisms of each cavity.

Table II gives the peak surface electric and magnetic fields reached before

inflection (that is, before degradation of Q_0) by each cavity in the three regimes. The data indicate that at 4.2°K and with the 2.5 μs pulse all of the cavities start to show increased losses at about the same field level, while for the 1.0 μs pulse the values are more scattered. The temperature of the bath seems to have little or no effect on the field at which the losses start to increase, while it has an effect on the hysteretic behavior (Fig. 25). The uniformity of values at the two temperatures might be associated with the exponentially decreasing heat capacity of Niobium as well as with the thermal relaxation time being much longer than the pulse length (adiabatic heating).

Few remarks should be made about these data: first, cavities which had remarkably different behavior in CW show very uniform properties in the pulsed case, indicating that the surface differences are not as crucially important. Second, the SLAC cavity treated for Indium removal, which greatly affected the CW properties, was not different from the others which were not treated. This fact implies that, at least up to the field levels where the Q_0 degradation starts to occur, the properties of the surface are not of great importance, and that cavities treated in different ways yield some common minimal result, a fact which is important from the point of view of applications: in this case extended structures might give, without any particular care, uniformly high fields.

For most cavities the inception of the Q_0 degradation was correlated with the onset of an extremely high-intensity x-ray emission. This fact led us first to believe that electron heating by impact on the walls was the primary cause of Q_0 degradation. One of the cavities, though, showed that, at the same field level for increased losses, the x-ray intensity was less than .01 of the emission for most other cavities, indicating that the Q_0 degradation might be ascribed to a more

fundamental phenomenon, although some of the details of the shape of the curve in the transition from the superconducting to the normal state can be related to the electron heating phenomenon and/or electron loading (Figs. 18 and 19).

Of the methods used to determine the inception of the Q_0 degradation (P_e vs P_i curves; observation of the more rapid decay of the transmitted power curve, both with a linear and a logarithmic amplifier; and, at 4.2°K, the increase in the boiloff which gives a sensitivity of $Q_0 \gtrsim 10^7$) we have been able to determine that the deviation from linearity of the P_e vs P_i curve gives the highest sensitivity. That is, we were able to see this deviation at a lower input power level than with any of the other methods. Also, by being an integral power method, it conveys much more information in a compact form. During the measurements, transmitted power curves, reflected gated power curves and x-rays were also constantly visually monitored for consistency and for possible deviations from normality.

During the initial phases of the testing of each cavity after assembly, sudden strong x-ray emission was observed as the cavity was going through field emission levels; in those instances the cavity was totally detuned and the x-ray survey meter always pegged during the spike, for rates in excess of 3 R/hr. The field emission behavior was quickly processed away in a matter of seconds and the cavities would not show again the sudden detunings.

Helium processing was done on the SLAC cavity at room temperature and at 77°K at which temperature peak surface fields of up to 130 MV/m can be reached with the present system. Several hours of processing did not appreciably alter the cavity behavior, indicating that all of the surface-property related field emission had been processed away during the beginning stages of the tests, by peak field

RF processing (Fig. 20).

The SLAC cavity also had a peculiar behavior which allowed us to independently calibrate the field levels in it. During the first tests at 4.2°K and 2.5 μs an x-ray emission peak appeared in the pulse-correlated x-ray detector. The peak would split into two peaks which would depart from one another as the power was increased, indicating an electron resonance phenomenon occuring during charge and discharge of the cavity. Figure 21 shows the transmitted field level correlated with the x-ray emission. The x-rays started to appear, according to our measurement procedure, at a field level of $\sim$ 35 MV/m and occurred only at that level, as the curves in Fig. 21 indicate. Past a certain field level, a third peak appears, which, from that point on is probably responsible for most of the integrated x-ray emission. For a 1 μs pulse length only the peak during discharge was present, indicating that the charging process was too fast to allow a resonant build-up of the phenomenon.

The same resonance peaks were observed at 77°K, at which temperature the Q_0 of $\sim$ 20,000 allowed the cavity to reach steady state during the pulse (Fig. 22). For that value of Q_0, β was very close to one, so that by standard measurement of Q_0, incident power during the pulse and β (as is done in CW) we were able to confirm the onset of the resonant x-rays at the same field level of 35 MV/m. This measurement gave an independent confirmation of the validity of the integral emitted power method.

The data taken at 2°K and 2.3°K indicate that the hysteretic cycles are due entirely on the efficiency with which heat is transferred from the cavity into the Helium bath: when the Helium is superfluid it is able to handle the increasing average heat load without a sudden discontinuous temperature increase of the

cavity's inner surface (Figs. 23-25). At higher temperatures, both in the normal and in the subcooled fluid conditions, the Helium bath is not able to remove the heat fast enough and sudden drops in emitted power are observed. The P_e vs P_i curve is not a rapidly varying function, up to the threshold for the hysteretic jump, of the heat removal rate, but it is a function of the Q_0 degradation and of the peak field effects. The amplitude of the jumps is instead a function of repetition rate, pulse length and of the energy stored at the moment of the sudden collapse in Q_0.

The value of the incident power at the end of the hysteretic cycle before superconductivity is restored is a measure of the heat transfer efficiency from the cavity into the Helium bath and it therefore constitutes a measurement of the thermal properties of the cavity and of the cavity-to-bath interface.

A few carbon resistor thermometers were placed at selected positions outside the cavity. No resistor could be placed close to the iris because of its inaccessibility. Nonetheless a test was performed at 4.2°K by checking the resistances of all the resistors while the cavity was in a normal state, past the hysteretic jump and while the He boiloff rate had substantially increased: none of the resistors' temperature had increased, indicating that the source of heat was the lower cavity surface or the iris. This behavior was expected due to the relative inaccessibility of the iris outer surface.

Once the P_e vs P_i curves deviate from linearity (Fig. 26) it is necessary to take into account the increased losses in order to determine the actual peak field reached. Figures 27 and 28 show how the field correction can be determined in first approximation, through the measurement of the deviation of P_e from linearity (ΔP_e) and the determination of the Q_0 for that deviation. The curves

were obtained by assuming that either the cavity is in a lower Q_0 condition throughout charging and discharging (continuous lines), or it has higher losses only during discharge (dashed line).

Figures 26 and 29 show the field levels reached in the cavities with the first order corrections. The SLAC cavity shows the full transition to the normal state.

Figure 30 shows the increase in losses as a function of peak surface field. In order to explain in detail the shape of the P_e vs P_i curve during the transition from superconductivity to normality, a more sophisticated nonlinear model for the losses will have to be developed. The details of the model, though, could be tested against actual measurements, and we can change the dissipation during the pulse by changing the pulse length. Other observable quantities will help in identifying the correct model which, in turn will give information on which critical field is being reached before total breakdown in a superconducting cavity.

6. Conclusions

The data taken on the pulsed behavior of several Nb cavities indicate that peak surface electric fields close to 70 MV/m can be reached without appreciable losses. This electric field corresponds to a peak surface magnetic of about 1300 O_e. The maximum fields reached seem to be almost independent of the external bath temperature but seem to vary with pulse length.

The fact that cavities which had extremely varied behavior during the CW tests instead showed very similar field levels for Q_0 degradation when pulsed, indicates that the properties tested via pulsed measurements are not necessarily the same as those tested in CW. This fact also is important because practical

applications of pulsed RF superconductivity would require much less strict quality control on the cavities than for the CW operation.

ACKNOWLEDGEMENTS

The authors would like to acknowledge the cooperation of the High Energy Physics Laboratory, Stanford University, in electron beam welding and firing the *Nb* cavities. The Low Temperature Material Research Laboratory of SLAC assisted in the Cryogenics Operations. We would like to thank Hank Deruyter (SLAC) for the development of the fixed-coupling system. Much of the credit for the experimental results go to Jerry Zamzow who assembled and kept in perfect working order the complex system and instrumentation used for the tests.

Several stimulating discussions with Perry B. Wilson gave us encouragement and advice in performing the tests and interpreting them.

DISCLAIMER

REFERENCES

1. T. Yogi, G. J. Dick, and J. E. Mercereau, Phys. Rev. Lett. 39, No. 13, 826-829 (1977).

2. J. B. Stimmel, Ph.D. Dissertation, Cornell University, 1978.

3. Z. D. Farkas, SLAC Note "Low-Loss, Pulsed-Mode Cavity Behavior," February 1983 SLAC/AP-15.

4. I. E. Campisi, Z. D. Farkas, H. Deruyter and H. A. Hogg, IEEE Trans. Nucl. Sci. NS-30, No. 4, 3306-3308 (1983).

5. I. E. Campisi, SLAC Memorandum, January 4, 1983.

   I. E. Campisi, SLAC Memorandum, January 25, 1983.

6. See M. Tigner and M. Padamsee in *Proceedings of the SLAC Summer School on High Energy Particle Accelerators*, AIP Conf. Proc. No. 105 (M. Month, Ed.), New York, 1983, p. 801.

7. H. Piel, paper presented at the 12th International Conference on High Energy Accelerator, Chicago, August 11-16, 1983.

Table I

Low-power, long-pulse test results on Nb cavities

Cavity	Temp (K)	Q_{0max}	E_{max} (MV/m)	Q_0 (E_{max})	Remark
SLAC	4.2	9.6 E7	5.8	9.0 E7	after firing
SLAC	1.3	2.3 E9	22.3	1.4 E9	after firing
SLAC	4.2	8.9 E7	7.2	8.6 E7	after In strip
SLAC	1.3	1.1 E9	13.4	1.0 E9	after In strip (present)
LF1	4.2	9.9 E7	17.3	7.2 E7	
LF1	1.3	5.4 E8	24.9	4.5 E8	$X = 150$ mR/hr
LF2	4.2	7.6 E7	4.2	5.1 E7	
LF2	1.3	6.0 E8	4.4	1.7 E8	
LF3	4.2	7.7 E7	8.3	5.8 E7	
LF3	1.3	3.0 E8	7.6	1.9 E8	
LF4	4.2	9.9 E7	14.8	7.0 E7	
LF4	1.3	8.0 E8	23.2	2.3 E8	$X = 150$ mR/hr
LF5	4.2	9.3 E7	9.2	7.7 E7	
LF5	1.3	1.1 E9	10.3	9.8 E8	

Table II

Summary of peak surface fields reached before degradation of Q_0

	4.2°K 2.5 μs			4.2°K 1 μs			1.4°K 1 μs		
CAVITY	PRF (PPS)	E_s (MV/m)	H_s (Oe)	PRF (PPS)	E_s (MV/m)	H_s (Oe)	PRF (PPS)	E_s (MV/m)	H_s (Oe)
SLAC	82	59	1120	40	68.4	1300	33	67	1280
LF1	82	56	1020	57	60.6	1100	33	58	1060
LF2	82	58	1060	50	58	1060	51	58	1060 (2.5 μs)
LF5	82	60	1090	51	67	1220	33	65	1180

Figure Captions

1. Reverse power versus time for a 2.5 μs RF pulse and for various Q_e.
2. Pulsed RF energy transfer efficiency versus external Q for two pulse lengths ($T_p = 1$ μs and $T_p = 2.5$ μs).
3. Gating of the emitted power to obtain the energy stored in the cavity.
4. Scheme of the emitted power measuring apparatus.
5. Simplified version of Fig. 4.
6. Transmitted power pulse through a logarithmic receiver.
7. Transmitted power pulse through a linear receiver.
8. X-ray detector output in phase with the RF pulse.
9. Cross section of original SLAC TM_{010} Nb cavity.
10. Modified SLAC cavity with removable cutoff tube.
11. Cross section of the *leapfrog* cavities (LF) adapted for fixed coupling operation.
12. Fixed coupling cavity assembly with transmission probe.
13. P_e vs P_i curve for the SLAC cavity ($T = 4.2$°K, $T_p = 1.25$ μs, PRF = 50 pps).
14. P_e vs P_i curve for the cavity LEAPFROG #5 ($T = 4.2$°K, $T_p = 1$ μs, PRF = 51 pps).
15. P_e vs P_i curve for the cavity LEAPFROG #2 ($T = 4.2$°K, $T_p = 2.5$ μs, PRF = 82 pps).

16. P_e vs P_f curve for the SLAC cavity ($T = 4.2°K$, $T_p = 1\ \mu s$, PRF = 32 pps).

17. P_e vs P_f curve for the cavity LEAPFROG #2 ($T = 2°K$, $T_p = 2.5\ \mu s$, PRF = 51 pps).

18. Comparison of P_e vs P_f curves for two cavities with very different x-ray output. Curve 1 had an x-ray emission $\sim$ 100 times smaller than curve 2. Both curves show deviation from linearity at the same P_e level (pulse width, repetition rate and temperature are the same).

19. Correlation of x-ray emission with P_e vs P_f curve for the high-emission cavity of Fig. 18.

20. Comparison of P_e vs P_f curves before (1) and after (2) Helium processing.

21. Correlation of transmitted field on x-ray emission during the pulse at 4.2°K for increasing (a $\rightarrow$ c) field levels.

22. Same as Fig. 21(b) at 77°K.

23. P_e vs P_f curve for LF1 (PRF = 51 pps, $T_p = 2.5\ \mu s$) at various temperatures. Note that the departure from linearity always occurs at the same P_e level. a) $T = 1.4°K$; b) $T = 1.7°K$; c) $T = 2.0°K$; d) $T = 2.2°K$; e) $T = 3°K$; f) $T = 77°K$.

24. P_e vs P_f curve for LF5 (PRF = 51 pps, $T_p = 1\ \mu s$) at various temperatures. a) $T = 1.4°K$; b) $T = 2.18°K$; c) $T = 2.3°K$; d) $T = 3°K$; e) $T = 3.5°K$.

25. Superposition of P_e vs P_f curves for LF1 just below (1) and above (2) the λ point. The two curves coincide up to the point of the hysteretic breakdown (a).

26. P_e vs P_f curve showing the fields reached as the Q_0 degrades. In parentheses are the first order approximation corrected values. Cavity LF5,

$T = 1.4°K$, PRF = 51 pps, $T_p = 1\mu s$.

27. Relation linking $\Delta P_e/P_e$ to Q_0 for the pulse lengths and Q_e indicated.

28. Peak surface electric field correction curves for a given Q_0 and for a peak incident power of 1 MW.

29. P_e vs P_i curve for two cavities. The SLAC (1) cavity shows the transition from superconducting to normal over wide range of field levels.

30. Average losses in the cavity as a function of peak surface electric field, for the curve of Fig. 26.

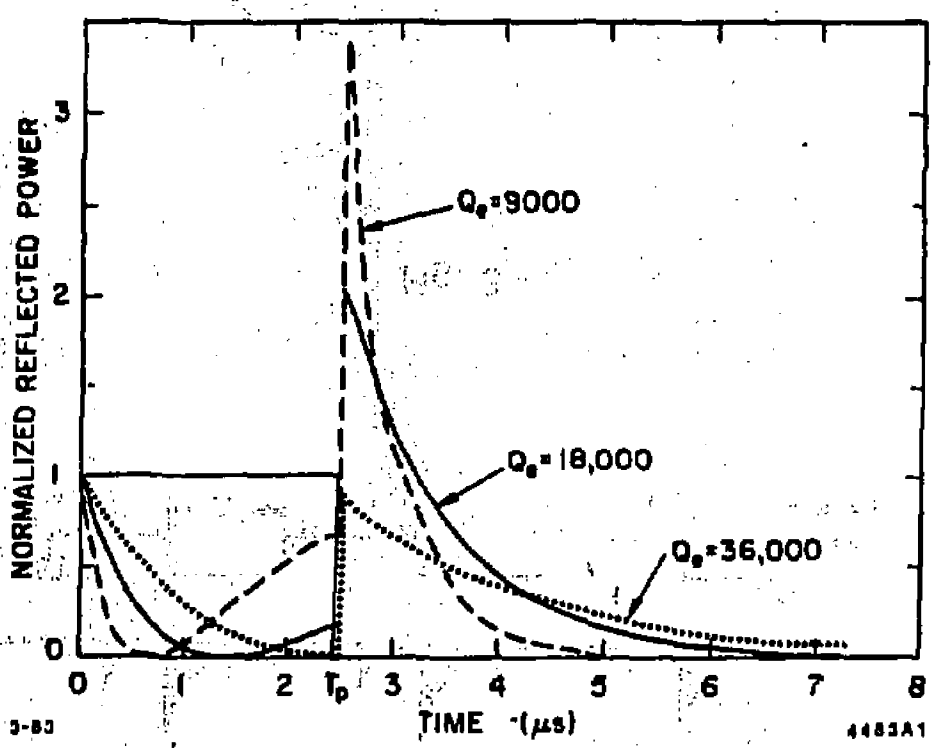
NORMALIZED REFLECTED POWER
3
2
1
0
Q_e=9000
Q_e=18,000
Q_e=36,000
0
1
2
T_p
3
4
5
6
7
8
TIME -(μs)
3-83
4483A1

Fig. 1

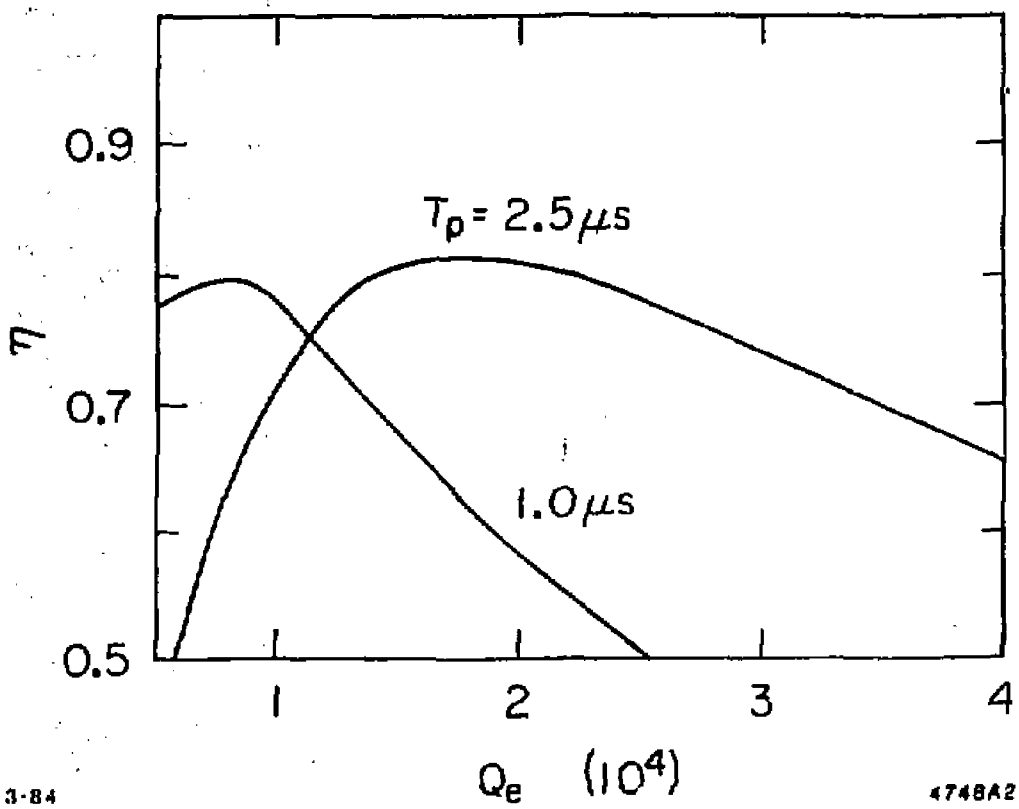

Fig. 2

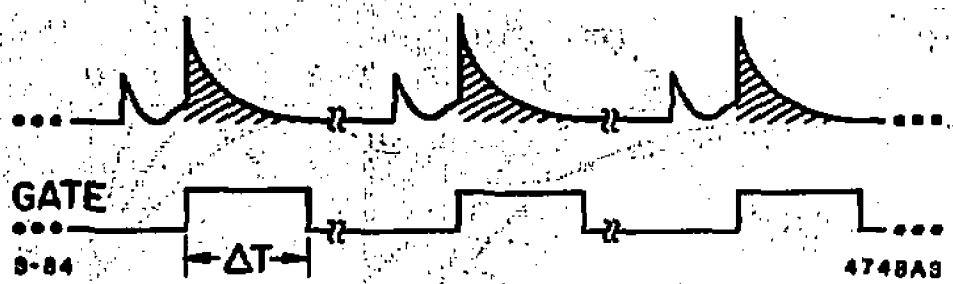

Fig. 3

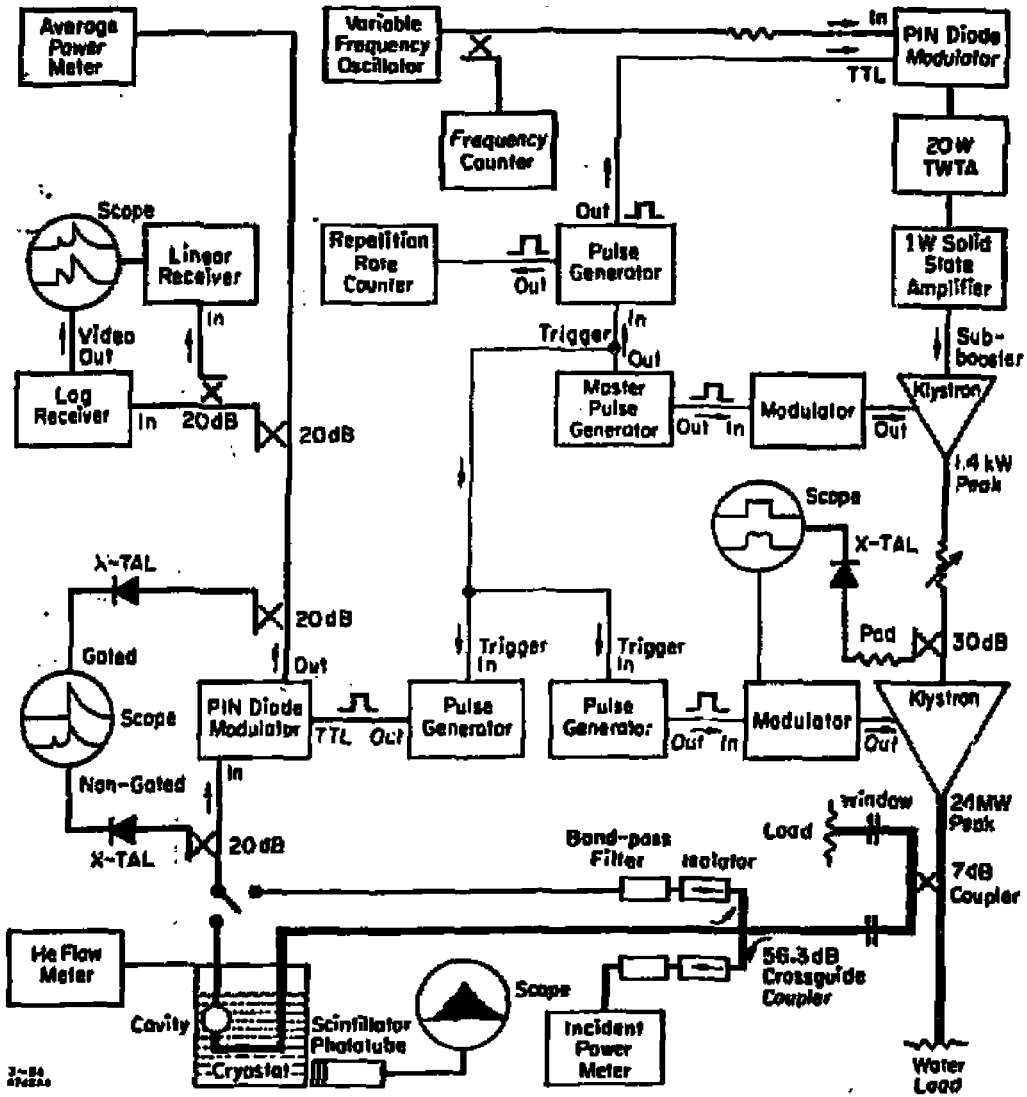
Average Power Meter
Variable Frequency Oscillator
In
PIN Diode Modulator
TTL
Frequency Counter
20W TWTA
Scope
Linear Receiver
Repetition Rate Counter
Out
Pulse Generator
1W Solid State Amplifier
Video Out
In
Trigger
In
Out
Sub-booster
Log Receiver
In
20dB
20dB
Master Pulse Generator
Out
In
Modulator
Out
Klystron
1.4 kW Peak
Scope
X-TAL
X-TAL
20dB
Trigger In
Trigger In
Pad
30dB
Gated
Out
Scope
PIN Diode Modulator
TTL
Out
Pulse Generator
Pulse Generator
Out
In
Modulator
Out
Klystron
Non-Gated
In
window
24MW Peak
X-TAL
20dB
Band-pass Filter
Isolator
Load
7dB Coupler
He Flow Meter
Cavity
Scintillator
Phototube
Cryostat
Scope
56.3dB Crossguide Coupler
Incident Power Meter
Water Load

Fig. 4

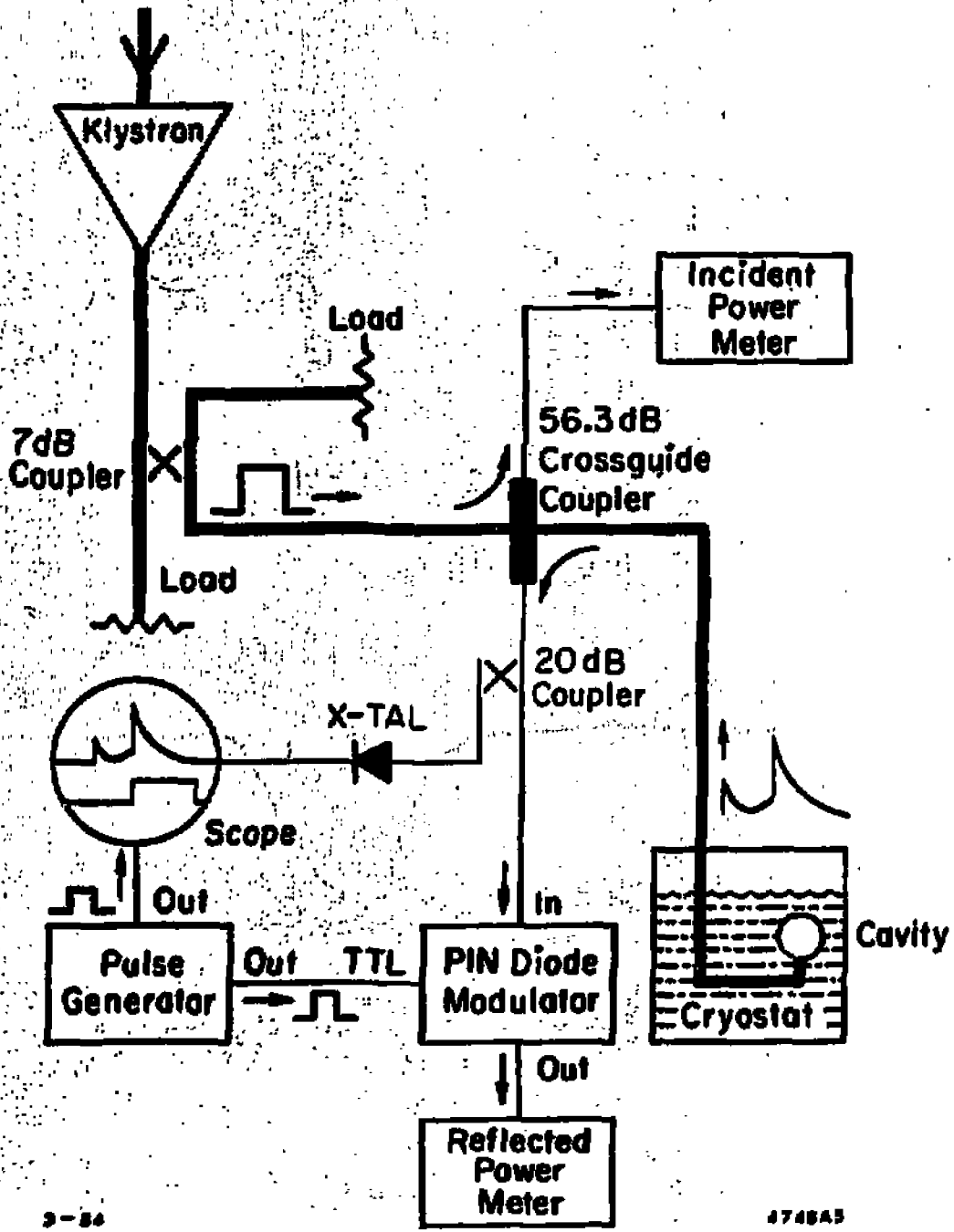
Klystron
Incident Power Meter
Load
56.3dB Crossguide Coupler
7dB Coupler
Load
20dB Coupler
X-TAL
Scope
Out
In
Cavity
Pulse Generator
Out
TTL
PIN Diode Modulator
Cryostat
Out
Reflected Power Meter
3-84
4748A5

Fig. 5

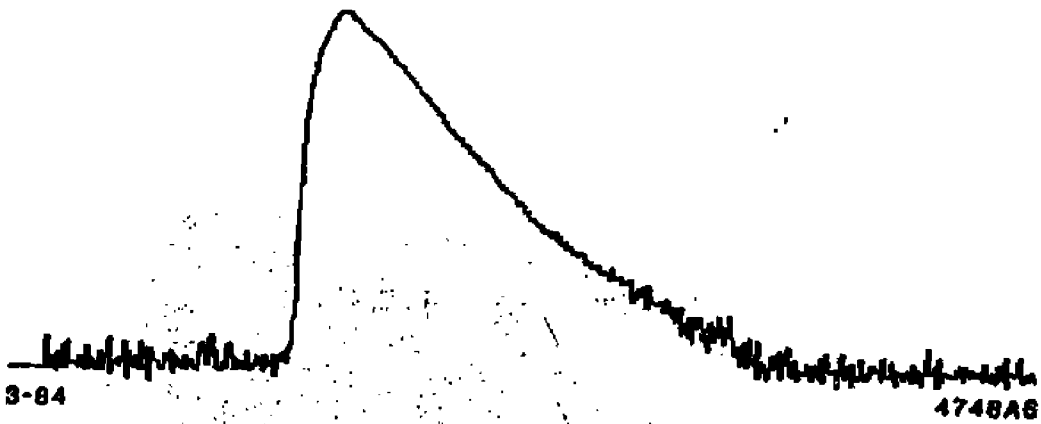

Fig. 6

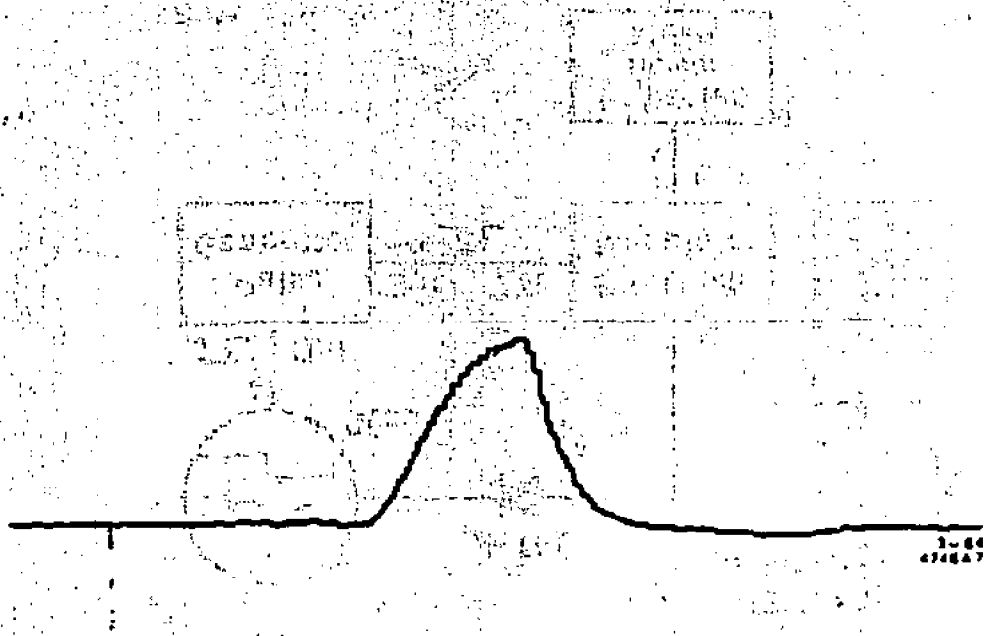

Fig. 7

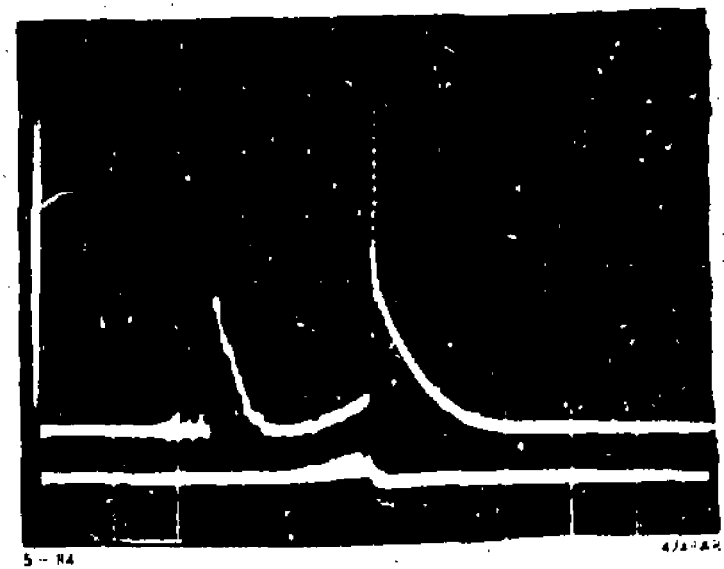

Fig. 8

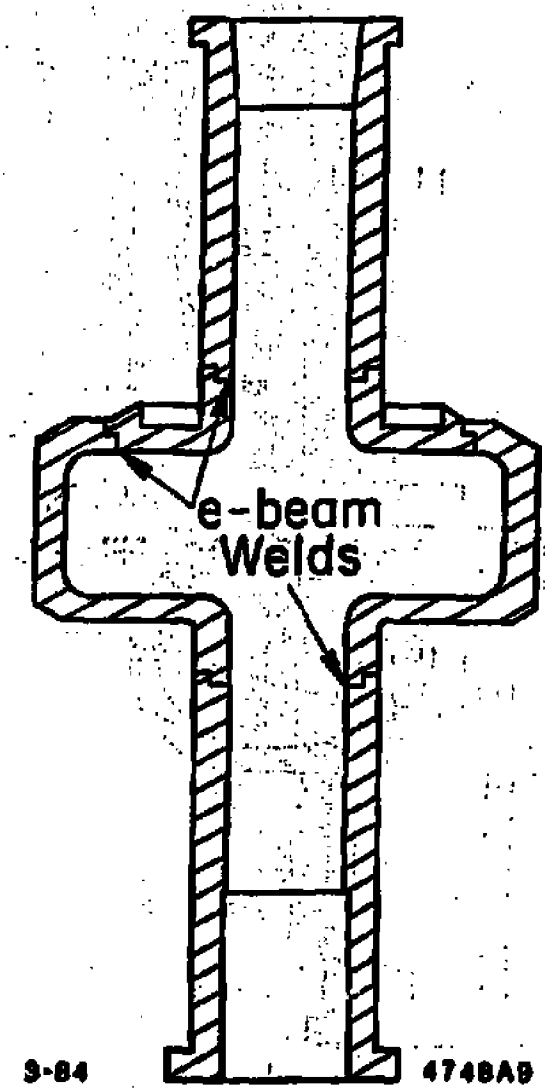

Fig. 9

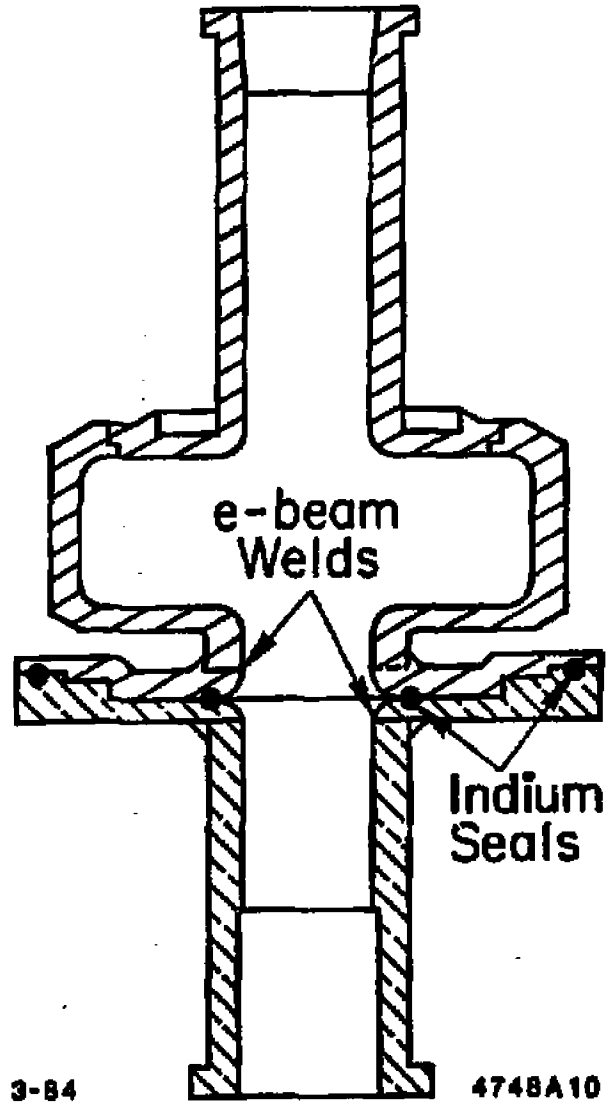

Fig. 10

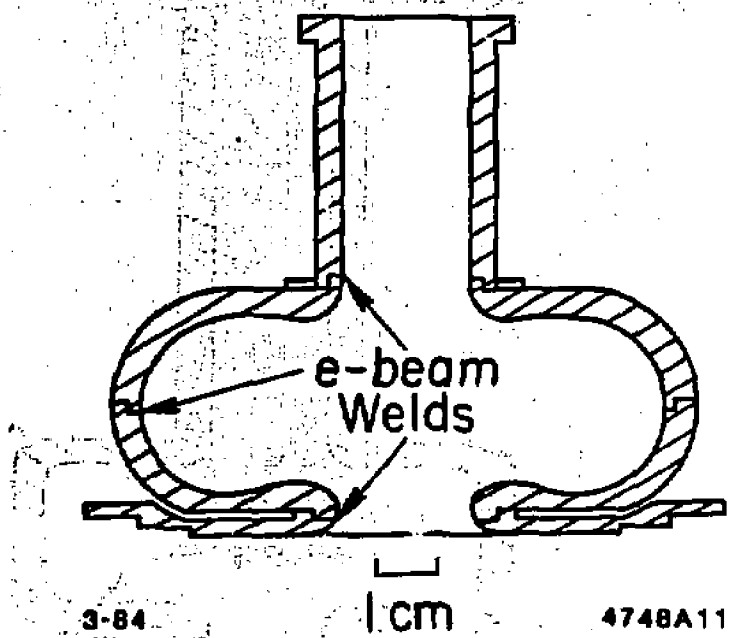

Fig. 11

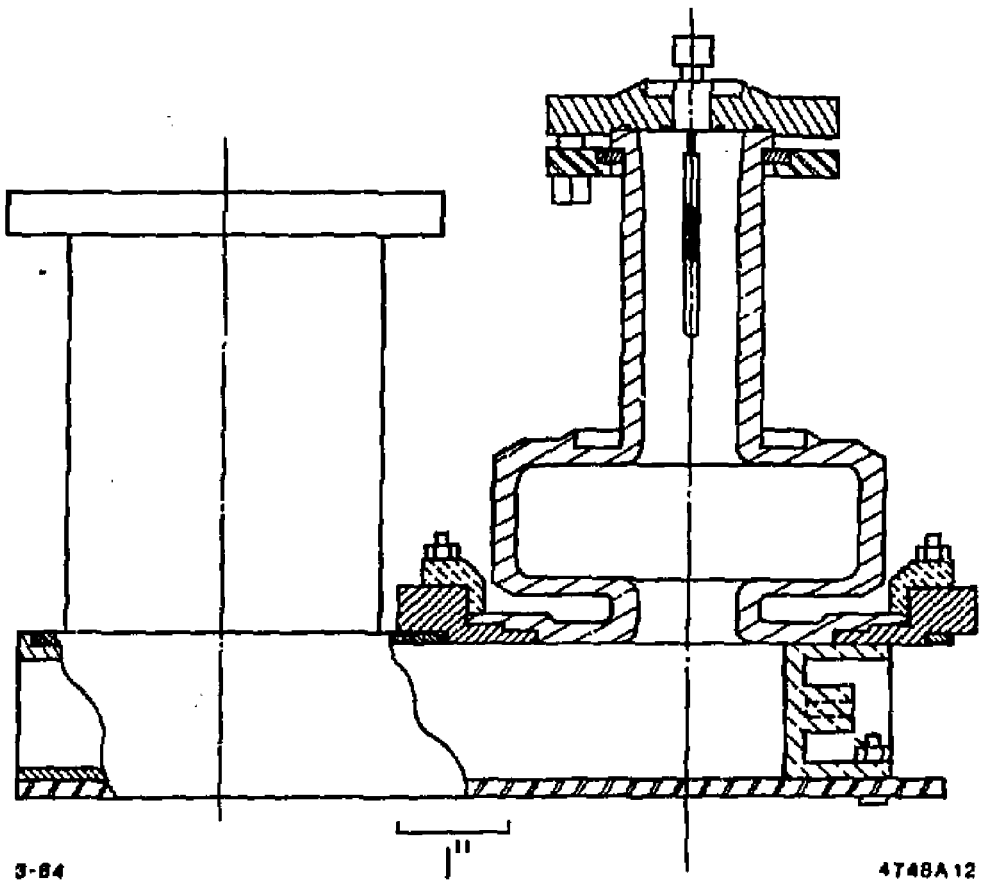

Fig. 12

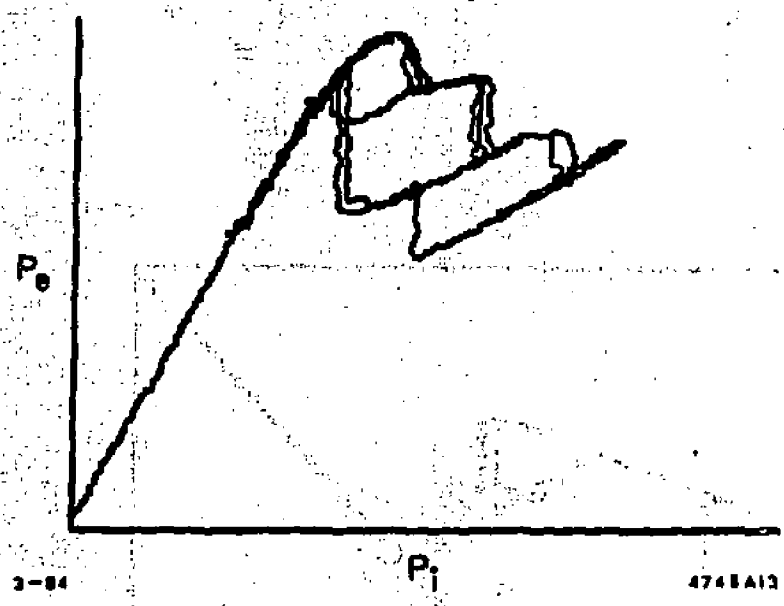

Fig. 13

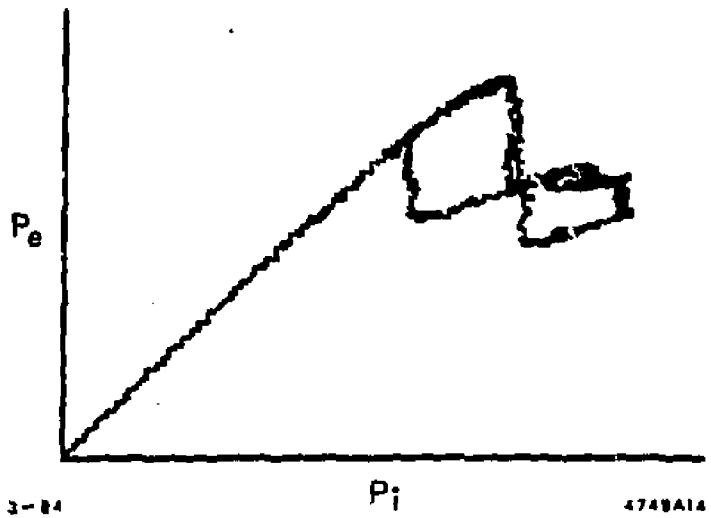

Fig. 14

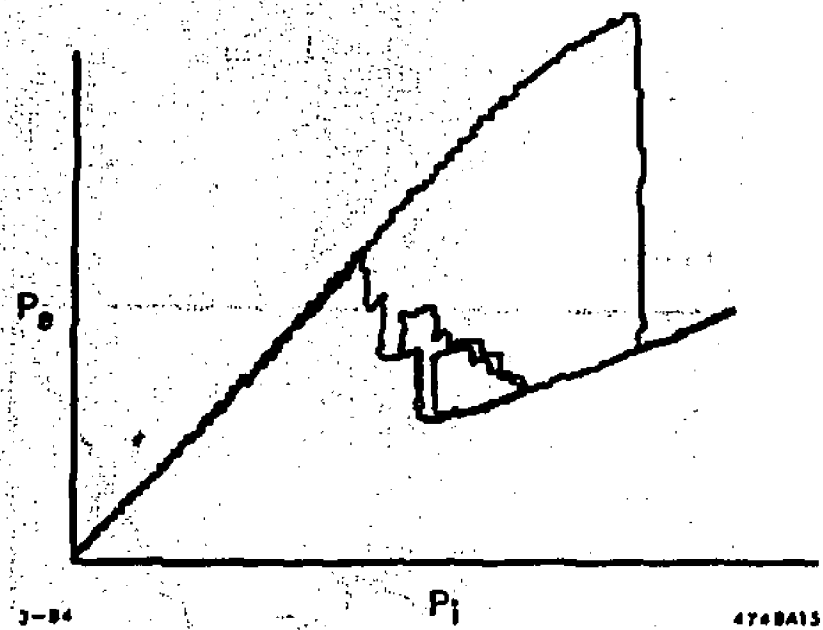

Fig. 15

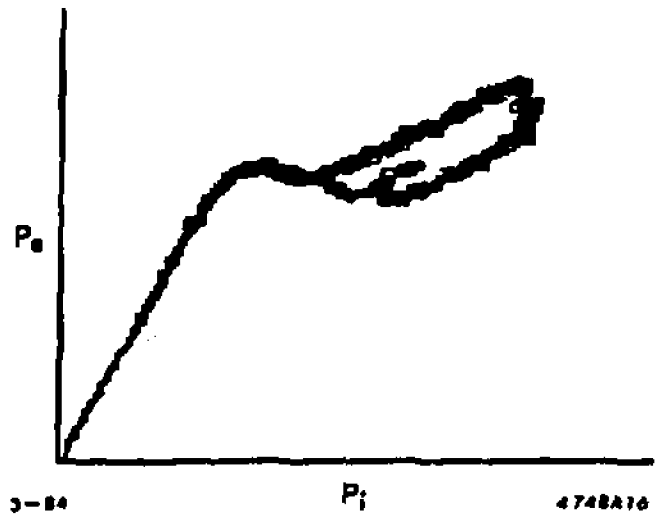

Fig. 16

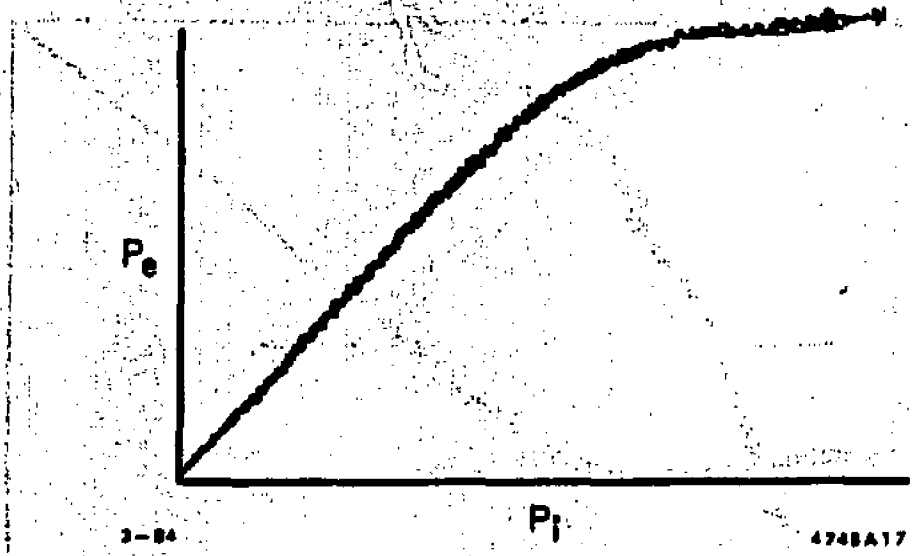

Fig. 17

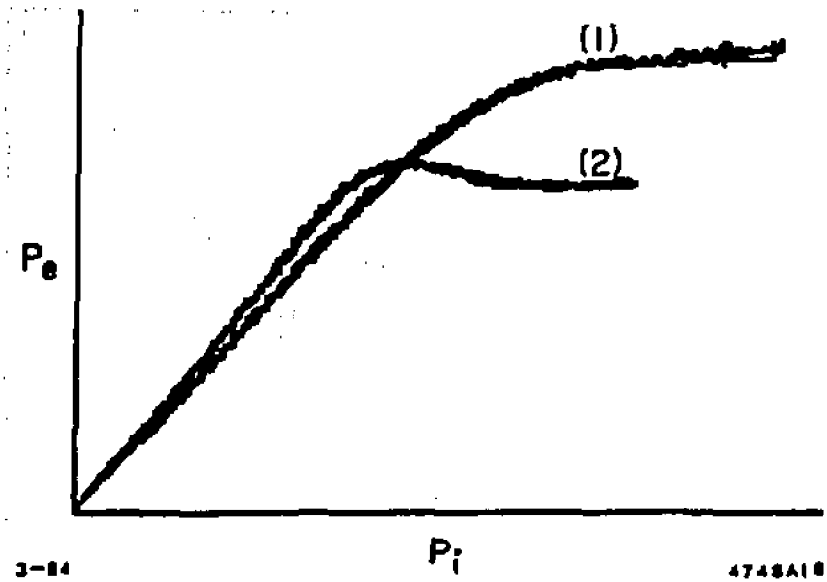

Fig. 18

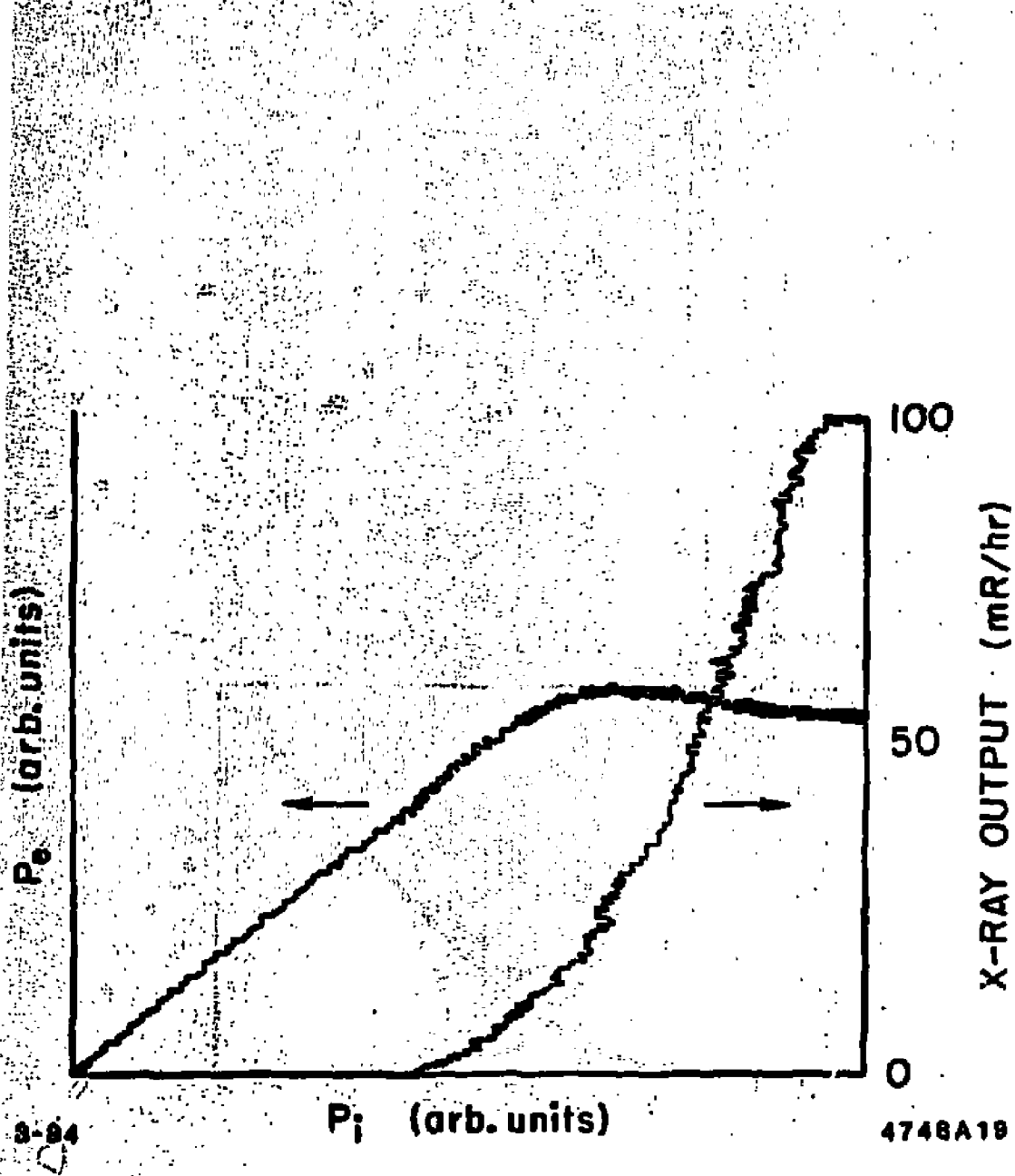
100
50
0
X-RAY OUTPUT · (mR/hr)
P_e (arb. units)
P_i (arb. units)
3-84
4746A19

Fig. 19

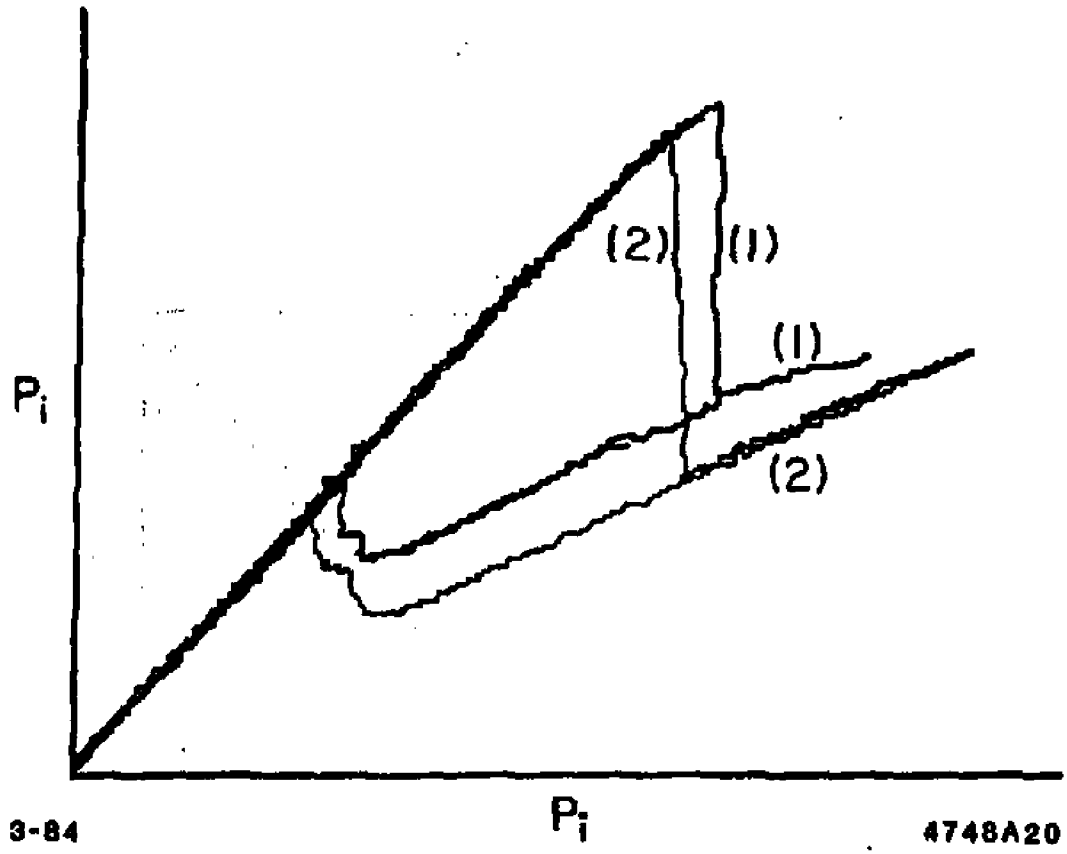

Fig. 20

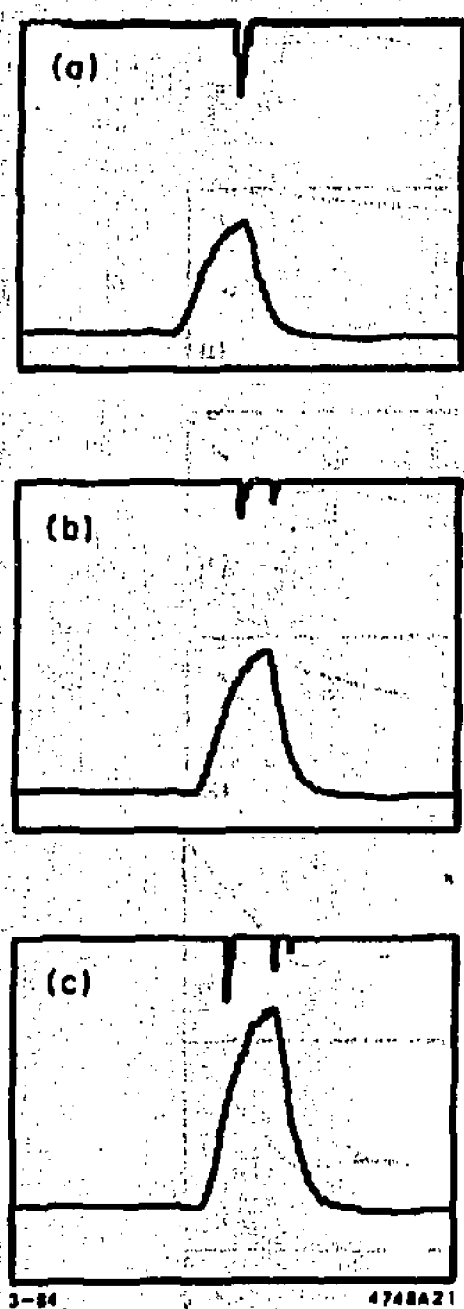

Fig. 21

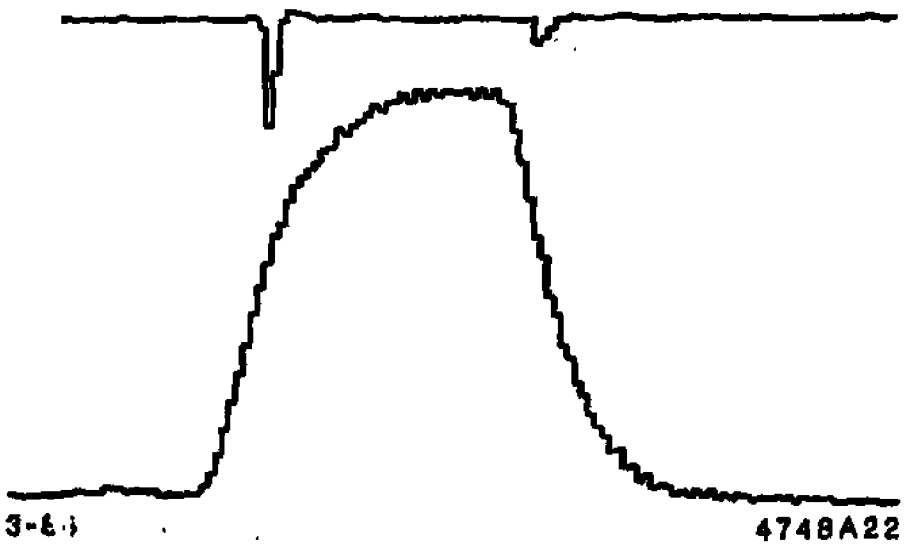

Fig. 22

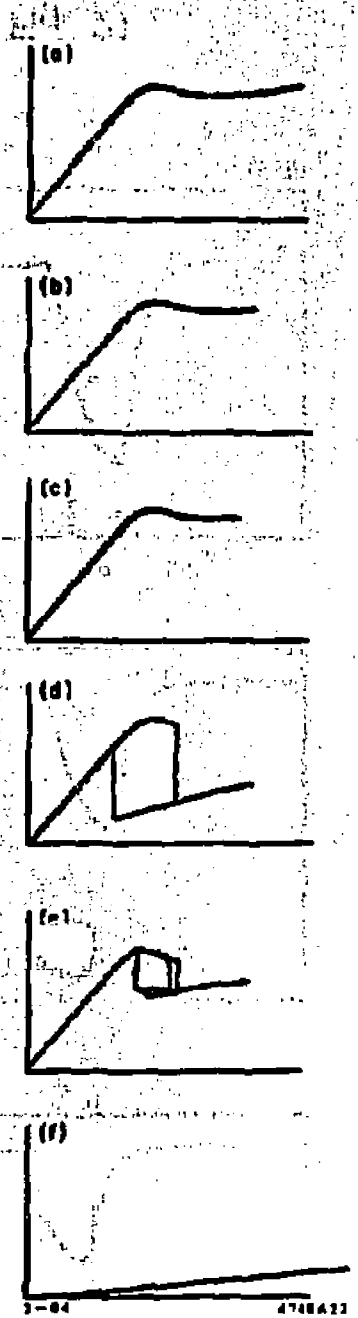

Fig. 23

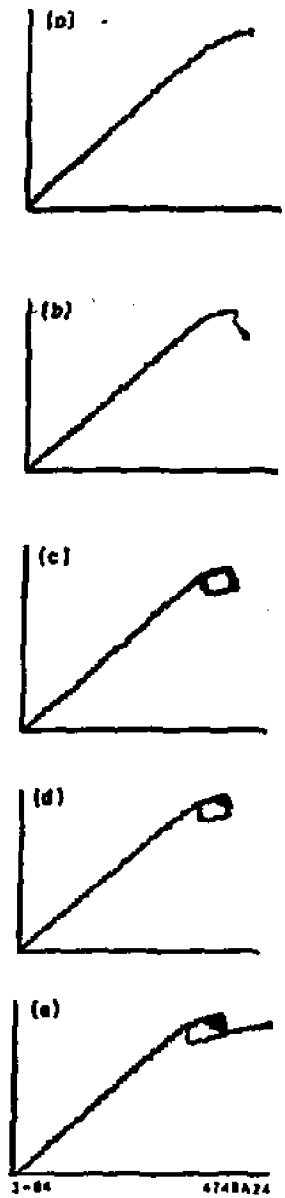

Fig. 24

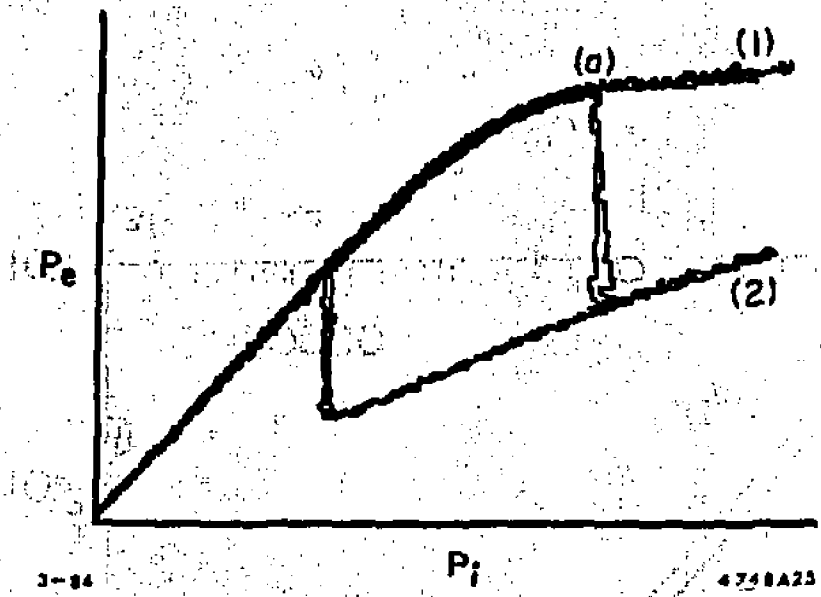

Fig. 25

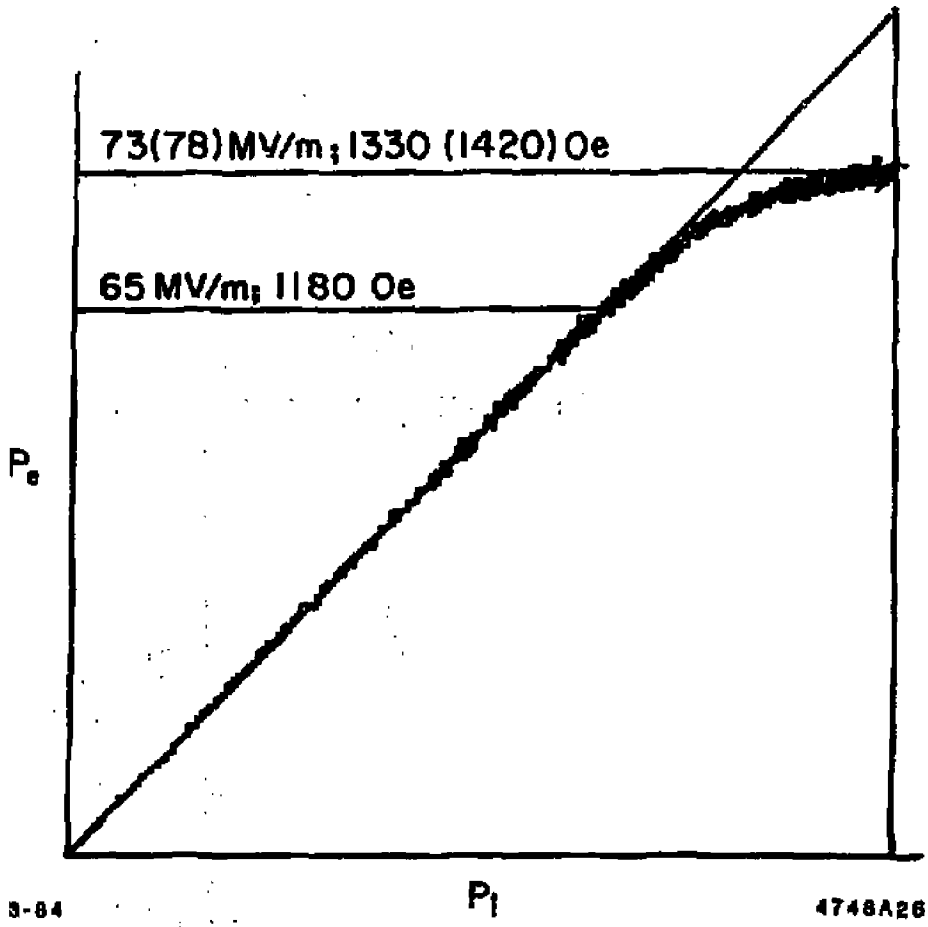

Fig. 26

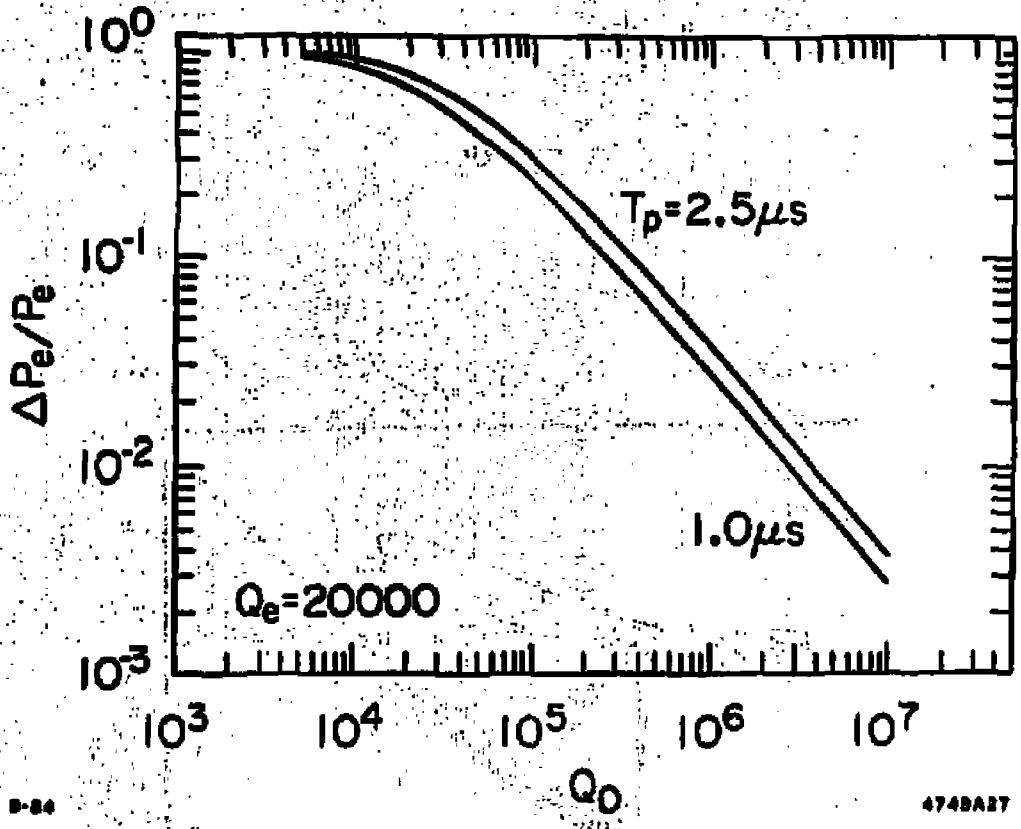
10^0
10^{-1}
10^{-2}
10^{-3}
$\Delta P_e/P_e$
T_p=2.5μs
1.0μs
Q_e=20000
10^3
10^4
10^5
10^6
10^7
Q_0
B-84
4749A27

Fig. 27

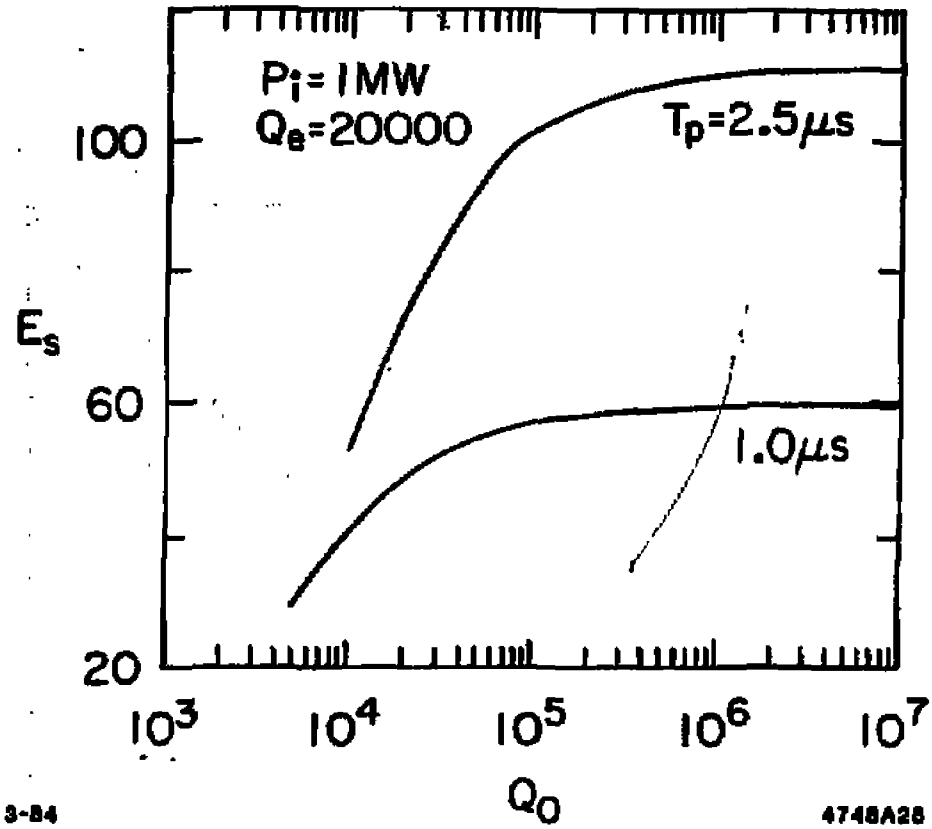
P_i = 1MW
Q_e=20000
T_p=2.5μs
1.0μs
100
60
20
E_s
10^3
10^4
10^5
10^6
10^7
Q_0
3-84
4748A28

Fig. 28

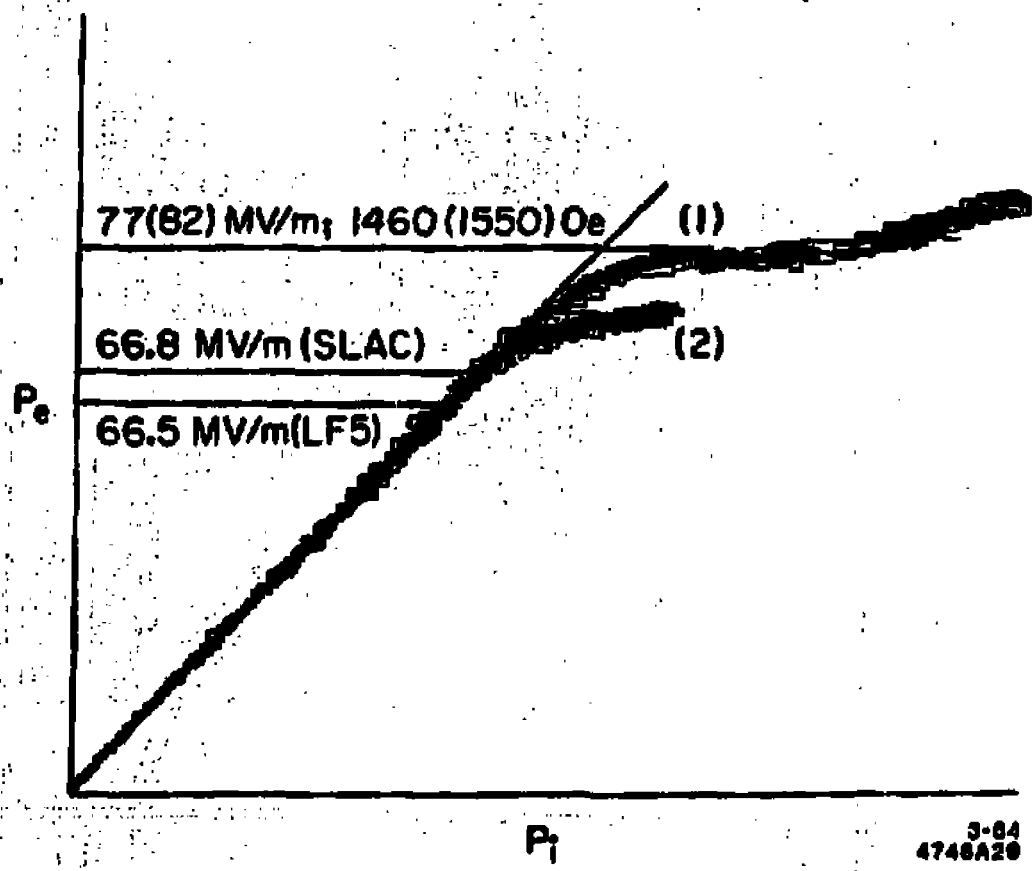
77(82) MV/m; 1460(1550) Oe
(1)
66.8 MV/m (SLAC)
(2)
66.5 MV/m(LF5)
P_e
P_t
3-84
4746A28

Fig. 29

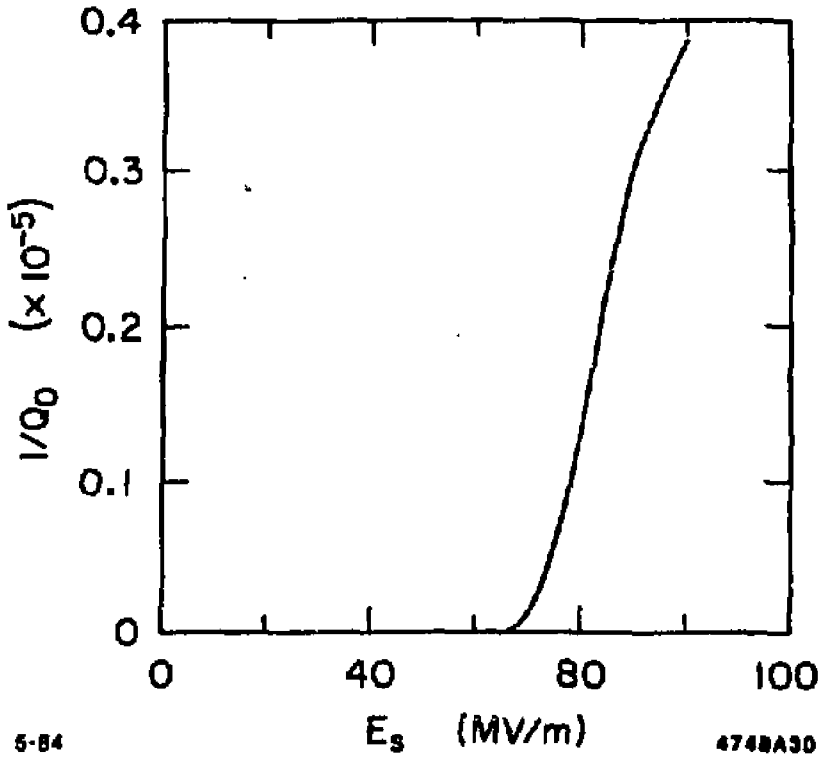

Fig. 30